International Journal of Robotics and Control Systems
Vol. 5, No. 1, 2025, pp. 86-104
ISSN 2775-2658
http://pubs2.ascee.org/index.php/ijrcs

# Optimizing Low-Voltage Ride-Through in DFIG Wind Turbines via QPQC-Based Predictive Control for Grid Compliance

Ahmed Badawi [a,1], Mostafa Soliman [a,2,*], I. M. Elzein [a,3], Walid Alqaisi [a,4]

[a] College of Engineering and Technology, University of Doha for Science and Technology, 24449 Arab League St, Doha, Qatar
[1] ahmed.badawi@udst.edu.qa; [2] mostafa.soliman@udst.edu.qa; [3] 360101973@udst.edu.qa; [4] walid.alqaisi@udst.edu.qa
* Corresponding Author

ARTICLE INFO

**Article history**
Received October 06, 2024
Revised November 26, 2024
Accepted December 05, 2024

**Keywords**
Wind Energy;
Model Predictive Control;
Power Converter;
Wind Energy Conversion System;
Doubly Fed Induction Generator;
Quadratically-Constrained Quadratic-Program (QCQP)

ABSTRACT

This paper introduces a novel Model Predictive Control (MPC)-based strategy to enhance Low-Voltage Ride-Through (LVRT) capability for wind turbines equipped with Doubly Fed Induction Generators (DFIGs). According to modern grid codes, grid-connected wind turbines must remain operational during voltage dips and support the grid by injecting both active and reactive power. However, voltage dips pose significant challenges for (DFIG)-based wind turbines because voltage dips can induce significant large inrush current in the rotor, potentially damaging the rotor converter. Conventional control methods employ proportional-integral (PI) controllers for rotor current regulation and crowbar circuits to protect the converter by diverting high rotor currents away from the converter when they exceed their safe limit. While effective in protecting the hardware, crowbar activation temporarily disconnects the rotor from control, leading to a loss of power injection capabilities and noncompliance with grid codes. To overcome these limitations, this paper proposes an MPC-based rotor current controller formulated as a Quadratically-Constrained Quadratic Programming (QCQP) optimization problem. This controller explicitly incorporates rotor current and voltage constraints while optimizing control performance during grid faults. MATLAB-based simulations for both low- and medium-voltage dips demonstrate the superiority of the proposed approach over conventional PI controllers. The results confirm that the MPC strategy ensures LVRT compliance without the need for a crowbar circuit, maintaining stability and improving performance during a wide-range of fault conditions.



## 1. Introduction

The adoption of Doubly-Fed Induction Generators (DFIGs) in Wind Energy Conversion Systems (WECSs) has become widespread in the market for medium-sized wind turbines [1]-[4]. DFIG-based wind turbines offer several advantages over other types. They allow for variable-speed operation, optimizing energy capture across different wind speeds. Additionally, they use a partially rated power electronic converter, typically around 30% of the total generated power, which helps reduce costs and

energy losses. These WECSs also provide high efficiency, lower harmonic distortion, and improved power quality [5].

Recently, there has been a noticeable shift towards the use of Permanent Magnet Synchronous Generators (PMSG) for wind power generation to increase output power and maximize the energy capture through the use of full-scale converter setups [6]-[9]. PMSM-based wind turbines offer a balance between generator size and maintenance requirements, by eliminating the necessity for individual gearboxes, achievable through a high number of pole pairs [10]-[12]. Comparative studies between PMSGs and DFIGs indicated a 40% reduction in failure rate for PMSGs at the preliminary operative stage [13]-[15]. The integration of fully scaled converters enables these systems to manage reactive power and improve grid connectivity. This separation from the grid enhances system resilience, allowing for better fault tolerance without additional hardware requirements [11], [16]. Furthermore, the WECS efficiency is superior when compared to other types of turbines [17]-[21]. Although the transition to PMSGs offers benefits such as reduced maintenance and improved efficiency [22], [23], DFIGs remain the dominant technology in wind power generation. This is despite the significant challenges they face, particularly in maintaining compliance with grid codes during faults.

Fig. 1 illustrates the integration of a DFIG-based WECS with a three-phase grid through two conversion stages. A wound rotor induction generator is used to convert the mechanical power captured by the wind turbine blades into electric fugal energy [20], [24]-[27]. The stator of the DFIG is directly connected to the grid, while the rotor is connected to the grid through a Rotor-Side Converter (RSC) and a Grid-Side Converter (GSC) [25], [28]-[31]. One of the main advantages of DFIGs is that the generator speed can be adjusted by controlling the rotor-injected power and frequency. This is achieved by using a power electronic converter rated at a fraction (approximately 30%) of the wind turbine's total rated power [31]-[35].

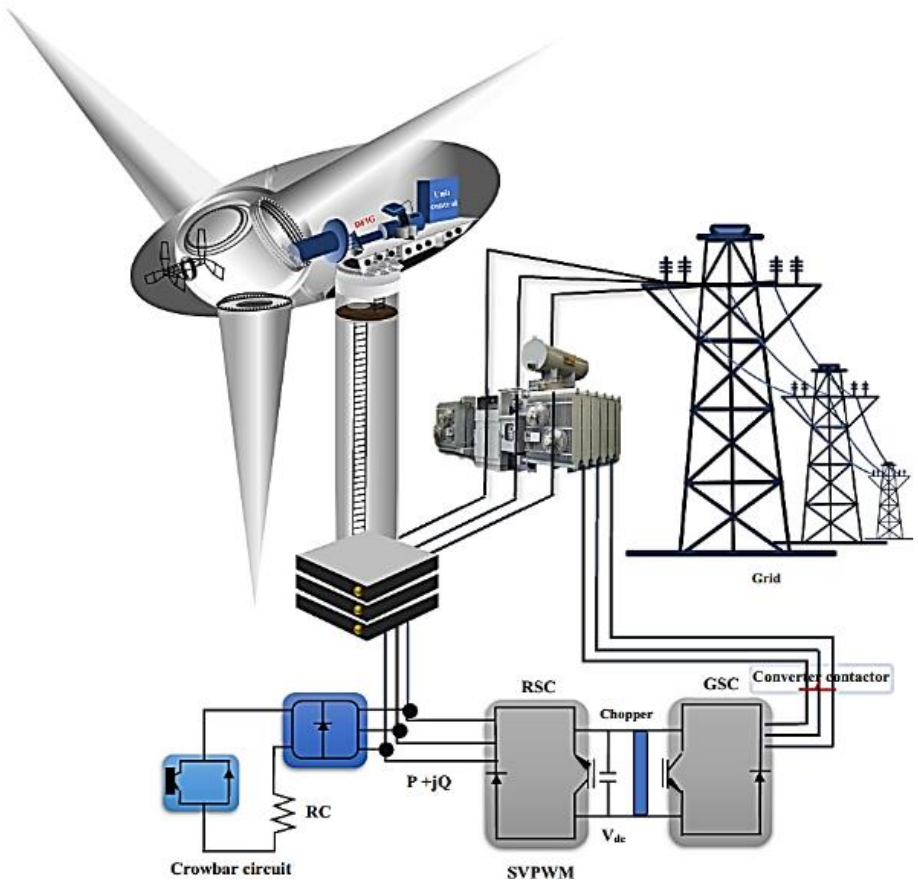


**Fig. 1.** Schematic diagram of the DFIG-based WECS

Fig. 2 represents the control system architecture of a DFIG-based wind turbine. At low wind speeds, the turbine controller adjusts the generator torque setpoint ($T_g^*$) to run the generator at its optimal speed, consequently maximizing the WECS efficiency. At high wind speeds, the turbine controller adjusts the pitch angle setpoint ($\beta^*$) to regulate the generator power and speed at their rated values. The RSC controller adjusts the rotor voltage ($v_r$) to control the generator torque and stator reactive power ($Q_s$), while the GSC adjust the GSC voltage ($v_C$) to control the DC link voltage ($V_{dc}$) and the GSC reactive power ($Q_{GC}$).

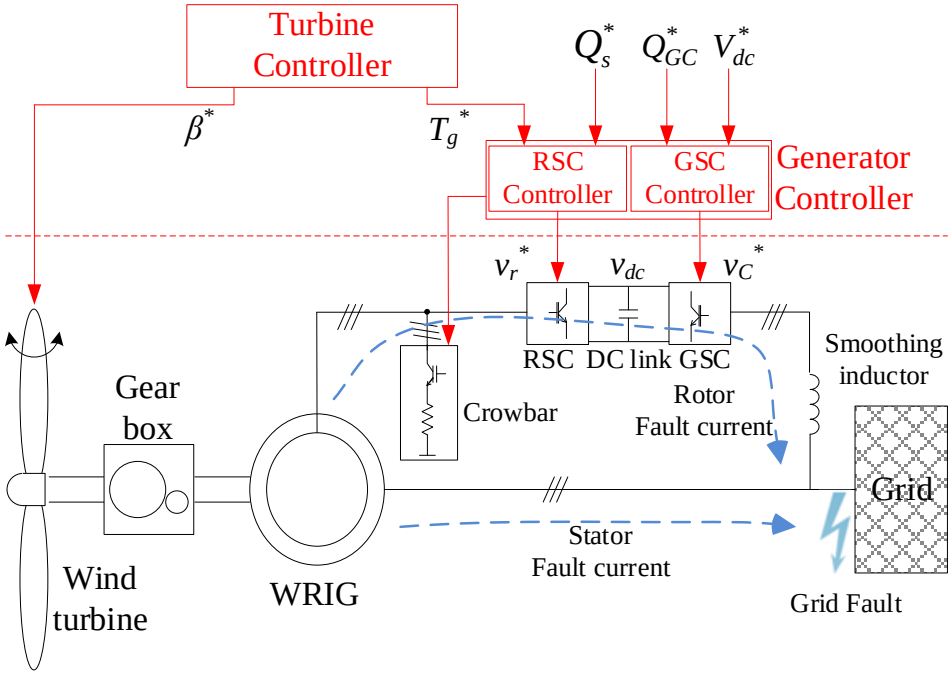


**Fig. 2.** Control system architecture of a DFIG-based wind turbine

The rapid expansion of wind energy and its integration into the electrical grid have presented various challenges related to stability, reliability, and functionality. As wind energy penetration levels increase, the LVRT requirement has been included in the grid codes of most countries [36]-[40]. The LVRT requirement mandates that wind farms remain connected to the grid with full control over their active and reactive power during certain voltage dips and fault durations. LVRT is essential for maintaining the stability of wind power plants; and ensuring they stay connected to the grid during voltage dips; to prevent outages [41]-[43].

Meeting the LVRT requirement for Doubly Fed Induction Generator (DFIG)-based wind turbines is a demanding task. As illustrated in Fig. 2, when a sudden voltage dip occurs at the DFIG terminals, significant currents flow from the DFIG's stator and rotor towards the fault, posing a risk of permanently damaging the power electronic converters (RSC and GSC), which are typically rated for only about 30% of the generator's full power capacity. To protect the converters from these high currents, protection devices such as a crowbar (Fig. 2) or a dynamic series resistance can be employed. Crowbar resistance is applied to divert the high currents away from the converters, while the dynamic series resistance is inserted in series with the rotor to limit the magnitude of the rotor current.

Recent LVRT requirements pose a significant challenge that impacts the design and control of power converters in DFIGs. Several studies have been conducted to assess the performance of various LVRT techniques on numerous WECSs during grid faults [44]-[50]. These techniques can be classified into hardware and software solutions. Section 2 will discuss and explain these techniques.

This paper proposes a novel Model Predictive Control (MPC) strategy to enhance the Low Voltage Ride Through (LVRT) capability of DFIG-equipped wind turbines. The strategy addresses challenges related to voltage dips and grid compliance. The proposed control strategy ensures that

rotor currents remain within safe limits and effectively mitigates disturbances caused by voltage dips and grid faults. Furthermore, the controller aims to improve the performance of reactive power injection, thereby aiding in voltage recovery after fault clearance.

The structure of this paper is outlined as follows: Section 2 presents the definitions and requirements related to LVRT. A summary of the DFIG model and its analysis is provided in Section 3. The proposed Model Predictive Control (MPC) controller for rotor current control is detailed in Section 4. Section 5 presents the simulation results, and Section 6 offers the concluding remarks of the paper.

## 2. Low-Voltage Ride-Through Capability

Grid-connected wind energy projects have experienced a surge in capacity, leading power utility operators to revise grid regulations and incorporate technical requirements for connecting wind power plants. The goal is to ensure grid consistency and reliability. While these regulations may differ from state to state, they share common foundations such as the ability to withstand low-voltage ride-through, limits on voltage and frequency variations, control of active power and frequency, management of reactive power, voltage regulation, and power factor control [51], [52]. Low-voltage ride-through (LVRT) allows wind energy systems to stay connected to the utility grid during voltage dips and grid disturbances, reducing power generation losses [53]. Grid codes are customized to meet specific needs, including variations in the severity of voltage dips and the allowable duration for wind turbines to remain connected to the grid [54], [55].

Fig. 3 illustrates the LVRT curve, with a specific emphasis on the code constructed by German utility operators, known as the E-ON code [56], [57]. It is essential for wind turbine generators to remain connected to the utility network during a grid dip when the line voltage remains above the specified limit shown in Fig. 3 a. Apart from meeting the requirement of active power, WECS must also inject reactive current, as indicated in Fig. 3 b, while ensuring that it does not exceed the converter's current limits. This injection of reactive power assists the utility in stabilizing the grid voltage. The amount of reactive power to be injected depends on the extent of the grid voltage dip, the level of reactive current present before the dip, and the grid's current rating. According to Fig. 3 b, LVRT capability should be activated when a voltage sag is detected below 90% of its nominal value. For a voltage sag between 50% and 90%, a reactive current of 2% should be provided for each 1% voltage dip. When a 50% drop in the grid voltage occurs, WECS will deliver a 100% reactive current [58]. As mentioned previously, strategies to improve LVRT capabilities in WECS can be classified into two categories: adjustments to control schemes and modifications to auxiliary hardware. Hardware techniques entail the utilization of external components such as chopper-controlled braking resistance  energy storage modules, and fault current limiters, as well as other alternatives [59]. Hardware solutions typically involve fewer complex controllers but are bulkier and more costly compared to software-based control alterations. Hence, this study focuses on the latter approach [60].

## 3. Modeling and Analysis of DFIG During Voltage Dips

In this section, the dynamic model of a DFIG and the analysis of its performance during voltage dips are summarized.

### 3.1. Induction Generator Model

A WRIG features a cylindrical rotor that rotates within a stationary stator core. Both the rotor and stator cores are constructed using laminated ferromagnetic sheets and are separated by a uniform air gap. The stator and rotor slots house three-phase symmetrical windings, which are evenly distributed along the inner circumference of the stator and the outer circumference of the rotor.

The modeling equations of the WRIG in terms of phase variables (a, b, and c) are usually hard to analyze and simulate because they contain time-varying coefficients. For this reason, the model is

much simplified using dq0 variable transformation which replaces the three-phase (a, b, and c) variables with a set of (d, q, and 0) variables associated with two orthogonal fictitious windings rotating at an arbitrary speed.

Using the dq0 variable transformation, the dynamics of a Wound Rotor Induction Generator (WRIG) are described by the following equations [61].

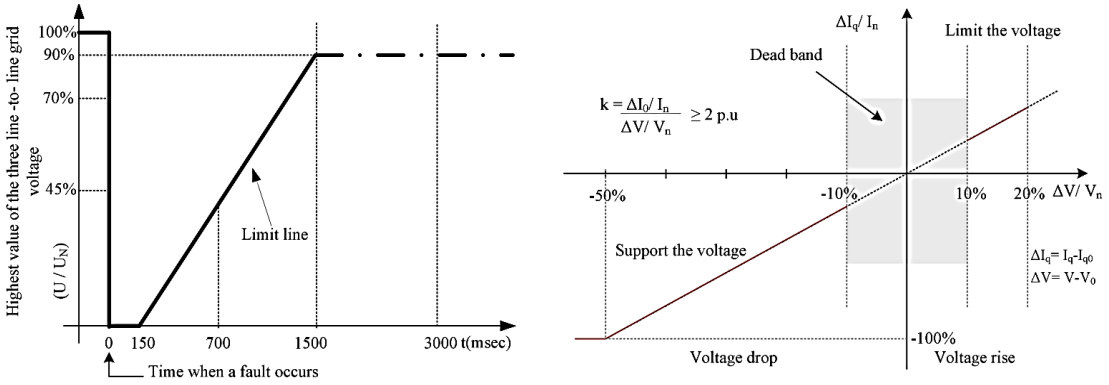


**Fig. 3.** LVRT requirement: (a) voltage limit curves; (b) reactive current injection during fault

$$\begin{aligned} v_{ds}^{a} &= i_{ds}^{a} r_s + p\lambda_{ds}^{a} - \omega_a \lambda_{qs}^{a} \\ v_{qs}^{a} &= i_{qs}^{a} r_s + p\lambda_{qs}^{a} + \omega_a \lambda_{ds}^{a} \\ v_{dr}^{a} &= i_{dr}^{a} r_r + p\lambda_{dr}^{a} - (\omega_a - \omega_r)\ \lambda_{qr}^{a} \\ v_{qr}^{a} &= i_{qr}^{a} r_r + p\lambda_{qr}^{a} + (\omega_a - \omega_r)\ \lambda_{dr}^{a} \\ \lambda_{ds}^{a} &= L_s i_{ds}^{a} + L_m i_{dr}^{a} \\ \lambda_{qs}^{a} &= L_s i_{qs}^{a} + L_m i_{qr}^{a} \\ \lambda_{dr}^{a} &= L_r i_{dr}^{a} + L_m i_{ds}^{a} \\ \lambda_{qr}^{a} &= L_r i_{qr}^{a} + L_m i_{qs}^{a} \end{aligned} \tag{1}$$

$$\begin{aligned} T_g &= P\left(\lambda_{ds}^{a} i_{qs}^{a} - \lambda_{qs}^{a} i_{ds}^{a}\right) = PL_m(i_{dr}^{a} i_{qs}^{a} - i_{qr}^{a} i_{ds}^{a}) \\ Q_s &= v_{qs}^{a} i_{ds}^{a} - v_{ds}^{a} i_{qs}^{a} \end{aligned} \tag{2}$$

Where;

$(d, q)$ = direct and quadrature axis

$(s, r)$ = stator/rotor quantities.

$(a, s, e, r)$ = arbitrary, stationary, synchronous rotate and rotors' reference frames, respectively.

$(v, i, \lambda, \omega_r, P)$ denote voltages, currents, flux linkages, rotor speed and the pair poles, respectively.

Equation (1) expresses the stator and rotor voltages in terms of the stator and rotor currents and flux linkages. The flux direct and quadrature stator and rotor flux linkages can be expressed in terms of the stator and rotor currents using (1). The generator electromagnetic torque and the stator reactive power can be calculated using (2).

The modeling equations in (1) and (2) can be compactly written using the space vector notation (e.g. $\vec{v}_s^{\,a} \stackrel{\text{def}}{=} v_{ds}^{a} + jv_{qs}^{a}$) as follow [61];

$$\vec{v}_s^{\,a} = r_s \vec{i}_s^{\,a} + p\vec{\lambda}_s^{\,a} + j\omega_a \vec{\lambda}_s^{\,a} \tag{3}$$

$$\vec{v}_r^a = r_r \vec{\imath}_r^a + p\vec{\lambda}_r^a + j(\omega_a - \omega_r)\,\vec{\lambda}_r^a \tag{4}$$

$$\vec{\lambda}_s^a = L_s \vec{\imath}_s^a + L_m \vec{\imath}_r^a \tag{5}$$

$$\vec{\lambda}_r^a = L_r \vec{\imath}_r^a + L_m \vec{\imath}_s^a \tag{6}$$

Using (3)-(6), it can be shown the rotor voltage expressed in the rotor reference frame (substitute $a$ with $r$) can be written as [61]:

$$\vec{v}_r^r = (r_r + p\sigma L_r)\vec{\imath}_r^r + \vec{e}_r^r \tag{7}$$

$$\vec{e}_r^r \overset{\text{def}}{=} \frac{L_m}{L_s} p\vec{\lambda}_s^r \tag{8}$$

Equation (8) can be regarded as the fundamental equation that relates the rotor voltage ($\vec{v}_r^r$), which can be controlled using the RSC, the rotor current ($\vec{\imath}_r^r$), and the internal (induced) rotor voltage ($\vec{e}_r^r$) [62]. It can be seen that large internal rotor voltages will cause large rotor currents. This will be discussed further in the next subsection.

### 3.2. DFIG at Full Voltage Dip

Under typical operating conditions, the stator voltage space vector (10) rotates continuously at a steady speed, $\omega_e$ = grid frequency, and remains at a constant magnitude $V_s$. Neglecting $r_s$, equation (11) for $\vec{\lambda}_s^s$ can be derived from equations (3) and (10), [61].

$$\vec{v}_s^s = V_s e^{j\omega_e t} \tag{9}$$

$$\vec{\lambda}_s^s = \frac{V_s}{j\omega_e} e^{j\omega_e t} \tag{10}$$

According to (9) and (11), the magnitude of the rotor internal voltage is denoted by (12), where the slip $s \coloneqq \frac{\omega_e - \omega_r}{\omega_e}$ [56]. The value of $s$ depends on the rotor speed. A typical range is $-0.3 \leq s \leq 0.3$. It can be concluded from (12), that the magnitude of the internal voltage $|\vec{e}_r^r|$ should be less than 30% of the stator voltage.

$$|\vec{e}_r^r| \approx V_s|s| \tag{11}$$

On the other hand, it can be shown that the magnitude of the internal voltage at the moment of a full voltage dip is given by (12), [61]. This indicates that the internal rotor voltage can be significantly higher than its normal operating value. This can cause very large rotor currents to flow through the rotor, which can pose significant risk to the power electronic converters.

$$\left|\vec{e}_{r,max}^r\right| \approx (1 - s)V_s \tag{12}$$

In the case of partial voltage dip, the magnitude of the internal rotor voltage will be between the extreme cases of no voltage dip as in equation (12) and full voltage dips as in equation (13). If no proper control is provided, even with small to medium voltage dips, the LVRT requirement imposed on the DFIG-based wind turbines might not be achieved. This will be addressed by the proposed MPC design in Section 4.

## 4. MPC Design of the Rotor Side Converter Controller

The use of MPC methods, as proposed by [63], offers numerous benefits for RSC control. MPC methods have the ability to handle constraints, allowing for the explicit incorporation of rotor current and voltage constraints within the controller. Additionally, these techniques enable effective feed-

forward compensation of deterministic disturbances, such as stator voltage. This facilitates quick rejection of stator voltage dips without waiting for the rotor currents to reach high values. Moreover, the MPC configuration is easy to implement by adjusting the prediction model used. This feature is advantageous as the dynamics of the controlled system, specifically the WRIG, change when the model parameters of the Doubly-Fed Induction Generator (DFIG) change.

The proposed MPC RSC control strategy is shown in Fig. 4. At each sampling time, the MPC controller solves an optimization problem using a prediction model as its main component. MPC has gained widespread acceptance in the industrial sector due to its high performance and control capabilities. Researchers have shown significant interest in MPC as it outperforms minimum variance (MV), generalized minimum variance (GMV), and pole placement (PP) techniques in managing processes with delays for extended periods or non-stable open-loop characteristics. MPC offers several advantages over structured PID controllers, such as the ability to handle constraints, robust control, and its straightforward application to complex, multivariable processes. Known as receding horizon control, MPC relies on various control techniques. The control signal is determined by minimizing the cost function. The controller's effectiveness depends on how accurately the system dynamics are captured by the input/output model used in the controller's design. MPC typically encompasses three key concepts:

1. Using a model to predict the future behavior of the system output.
2. Calculating a control sequence to optimize performance index metric.

The WRIG model, represented in a stator voltage-oriented reference frame rotating at synchronous speed, can be found in equations (14)-(17). Here, the control input is denoted as $u \stackrel{\text{def}}{=} [v_{dr}^e \quad v_{qr}^e]^T$ (input control), the state vector as $x = [i_{ds}^e \quad i_{qs}^e \quad i_{dr}^e \quad i_{qr}^e]^T$,the measurable disturbance as $d \stackrel{\text{def}}{=} [v_{ds}^e \quad v_{qs}^e]^T$ and the output controlled $z \stackrel{\text{def}}{=} [i_{dr}^e \quad i_{qr}^e]^T$. This model is derived by removing the flux linkage of the stator and rotor in equation (1).

$$\begin{aligned} \dot{x} &= \tilde{A}x + \tilde{B}u + \tilde{B}_d d \\ z &= C_z x \end{aligned} \tag{13}$$

$$\tilde{A}(u_{DSR}) = \begin{bmatrix} -\frac{r_s}{\sigma L_s} & (\omega_e + \frac{\omega_r L_m^2}{\sigma L_s L_r}) & \frac{r_r L_m}{\sigma L_s L_r} & \frac{\omega_r L_m}{\sigma L_s} \\ -(\omega_e + \frac{\omega_r L_m^2}{\sigma L_s L_r}) & -\frac{r_s}{\sigma L_s} & -\frac{\omega_r L_m}{\sigma L_s} & \frac{r_r L_m}{\sigma L_s L_r} \\ \frac{r_s L_m}{\sigma L_s L_r} & -\frac{\omega_r L_m}{\sigma L_r} & -\frac{r_r}{\sigma L_r} & (\omega_e - \frac{\omega_r}{\sigma}) \\ \frac{\omega_r L_m}{\sigma L_r} & \frac{r_s L_m}{\sigma L_s L_r} & -(\omega_e - \frac{\omega_r}{\sigma}) & -\frac{r_r}{\sigma L_r} \end{bmatrix} \tag{14}$$

$$\tilde{B} = \begin{bmatrix} -\frac{L_m}{\sigma L_s L_r} & 0 \\ 0 & -\frac{L_m}{\sigma L_s L_r} \\ \frac{1}{\sigma L_r} & 0 \\ 0 & \frac{1}{\sigma L_r} \end{bmatrix}, \tilde{B}_d = \begin{bmatrix} \frac{1}{\sigma L_s} & 0 \\ 0 & \frac{1}{\sigma L_s} \\ -\frac{L_m}{\sigma L_s L_r} & 0 \\ 0 & -\frac{L_m}{\sigma L_s L_r} \end{bmatrix} \tag{15}$$

$$C_z = [0_{2\times 2} \quad I_2] \tag{16}$$

By discretizing equations (14), we can obtain discrete time models as depicted in equation (18).

$$\begin{aligned} x(k+1) &= Ax(k) + Bu(k) + B_d d(k) \\ z(k) &= C_z x(k) \end{aligned} \tag{17}$$

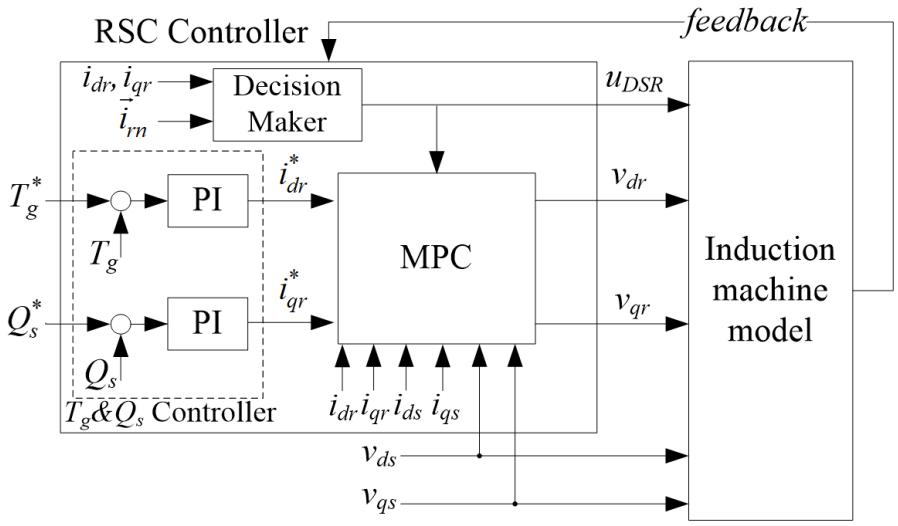


**Fig. 4.** Proposed control approach

The rotor currents are accurately tracked and maintained within safe boundaries by utilizing the Quadratically Constrained Quadratic Program (QCQP) presented in equations (19)-(22).

$$\min_{\substack{\forall \Delta u(k+j) \\ j=0,..,N_c-1}} \sum_{j=1}^{j=N_p} \left\| e^i(k+j) \right\|_Q^2 + \sum_{j=0}^{j=N_c-1} \|\Delta u(k+j)\|_R^2 + \rho\varepsilon^2 \tag{18}$$

Subject to:

Prediction model equations in (18).

$$\|u(k+j)\|_2^2 \leq V_{r,max}^2, \qquad j = 0, 1, \dots, N_c - 1 \tag{19}$$

$$\|z(k+j)\|_2^2 \leq I_{r,max}^2 + \varepsilon, \qquad j = 1, 2, \dots, N_p \tag{20}$$

$$\varepsilon \geq 0 \tag{21}$$

Where;

$N_p$ = prediction horizon,

$N_c$ =control horizon,

$$e(k) \stackrel{\text{def}}{=} r(k) - z(k) = \ Tracking\ error \tag{22}$$

Equation (24) represents weights $Q$ and $R$. The control moves, $\Delta u(k)$, is defined as $u(k) - u(k-1)$. The definitions $\|p\|_2^2 \stackrel{\text{def}}{=} p^T p$ and $\|p\|_M^2 \stackrel{\text{def}}{=} p^T M p$ are used in (19), (20) and (21).

$$Q = \begin{bmatrix} q_1 & 0 \\ 0 & q_2 \end{bmatrix}, R = \begin{bmatrix} r_1 & 0 \\ 0 & r_2 \end{bmatrix} \tag{23}$$

The QCQP described in (19)-(23) is an optimization problem where the objective function and constraints are quadratic in nature. Both the objective function and the constraints are convex; therefore, it can be solved using efficient numerical methods. QCQP can be widely found in signal processing, finance, control systems, and machine learning applications. Efficient Semi-Definite Program solvers exists to solve the QCQP [61], [64]. In this paper, SEDUM solver will be used.

There are other options to solve an approximate version of the QPQC in (19)-(23). One option is to approximate the quadratic constraints in equations (25) and (26) by utilizing two polytopes. In this

case, the QPQC in equations (19)-(23) can be approximated by the QP in equations (25)-(26), where 1 represents a vector entirely composed of 1, and $H_v$, $H_i$,$h_v$, and $h_i$ can be readily obtained from the polytope vertices. Quadratic constraints on the rotor voltage and the rotor current shown in Fig. 5.

$$\min_{\substack{\forall\, \Delta u(k+j) \\ j=0,..,N_c-1}} \sum_{j=1}^{j=N_p} \left\| e^i(k+j) \right\|_{Q^i}^2 + \sum_{j=0}^{j=N_c-1} \| \Delta u(k+j) \|_{R^i}^2 + \rho \varepsilon^2 \tag{24}$$

The equations in (19) are subject to the prediction model.

$$H_v u(k+j) \leq h_v, j = 0,1, \dots, N_c - 1 \tag{25}$$

$$H_i z(k+j) \leq h_i + \varepsilon 1, j = 1,2, \dots, N_p \tag{26}$$

$\varepsilon \geq 0$ as mentioned in equation (22).

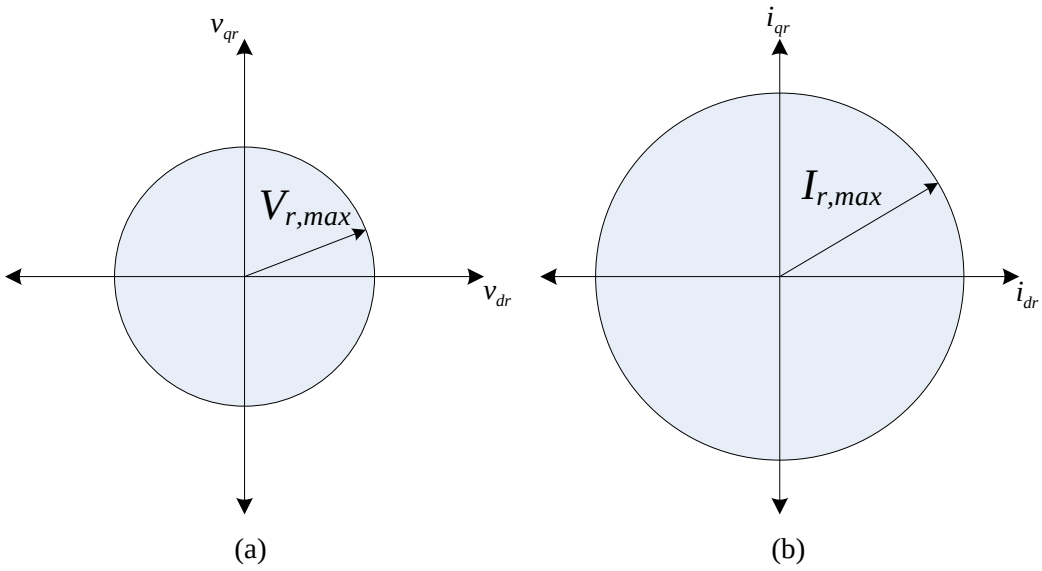


**Fig. 5.** Quadratic constraints on the rotor voltage (a) and the rotor current (b). The figure is shown for a typical case where $V_{r,max} < I_{r,max}$ when expressed as per-unit quantities

The QP in equations (22) and (26) can be addressed using two different MPC implementations. The first method involves the utilization of a QP solver, such as QPC [65], to resolve the optimization issue in equations (25)-(26) at every individual sampling time. This method is known as MPC_QP. The second approach is explicit MPC which involves solving the QP offline for all feasible initial states of a specific group of interest. In the work by [66], it was demonstrated that the explicit solution of the QP's can be computed. Explicit MPC controllers are computed through the Multi-Parametric Toolbox (MPT) [67]. This method is defined as $\text{MPC}_{\text{EXP}}$.

## 5. Simulation Results

In this section, two different types of faults have been applied to examine the performance of the MPC controller compared with the baseline PI controller. The simulation will study two cases: Case1 involves a small voltage dip of 0.2pu, and case 2 involves a medium voltage dip of 0.5pu. In each case, we will examine the rotor current, rotor voltage, and reactive power.

### 5.1. Small Voltage Dip

A small voltage dip is applied to the DFIG wind turbine. Both the MPC controller and the baseline PI controllers were simulated, and their responses are summarized in this subsection. Fig. 6 and Fig.

7 show the rotor current and voltage using the proposed MPC controller when a small voltage dip of 0.2pu is applied. Fig. 7 and Fig. 8 show the rotor current and voltage using the baseline PI controller when a small voltage dip of 0.2pu is applied.

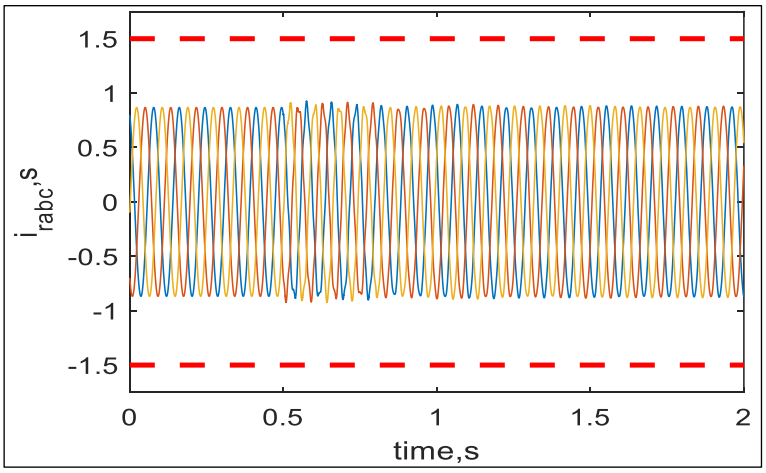


**Fig. 6.** Three-phase rotor current response using the proposed MPC controller during a small voltage dip

The reactive power was observed to evaluate the power quality using the MPC controller. Fig. 6 illustrates the application of the MPC controller for controlling the stator current during small voltage dips. The proposed MPC controller is implemented on the DFIG to mitigate small voltage dips. It can be seen that the signal remains at the operational level. The proposed MPC controller demonstrates high efficiency performance and maintains stable current at the nominal value ($I_{a,b,c}$= 0.85pu).

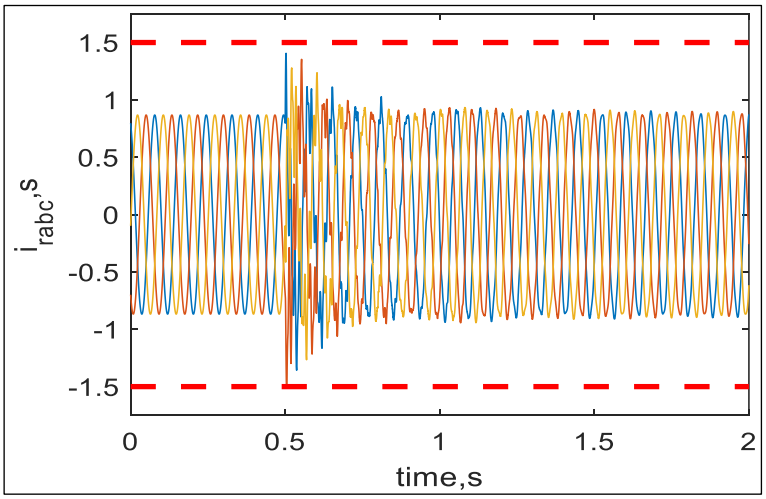


**Fig. 7.** Three-phase rotor current response using the baseline PI controller during a small voltage dip

Fig. 7 shows the application of a PI controller for the stator current based on small voltage dips. In this figure, the PI controller is applied to the same voltage dip profile to analyze the inrush current behavior of the DFIG. It can be observed from the figure that the inrush current reaches 1.4 pu, while the stable signal without sag ranges from 0.85 to 0.85 pu. Although the injected current is lower than the rotor current magnitude of ±1.5, it is still relatively high compared to Fig. 7, which demonstrates the effectiveness of the proposed system.

Fig. 8 represents the applied MPC controller for the stator voltage-based small dip voltage. The figure illustrates the dip in voltage after the MPC controller is applied. It is evident that the dip in stator voltage is short-lived, lasting for only 0.25 seconds. The fluctuation is contained within the acceptable range of rotor voltage limit (-0.5 to 0.5 Vpu). The MPC controller exhibits a rapid response

in adjusting the three-phase stator voltage to maintain the balance of the total power of the induction generator.

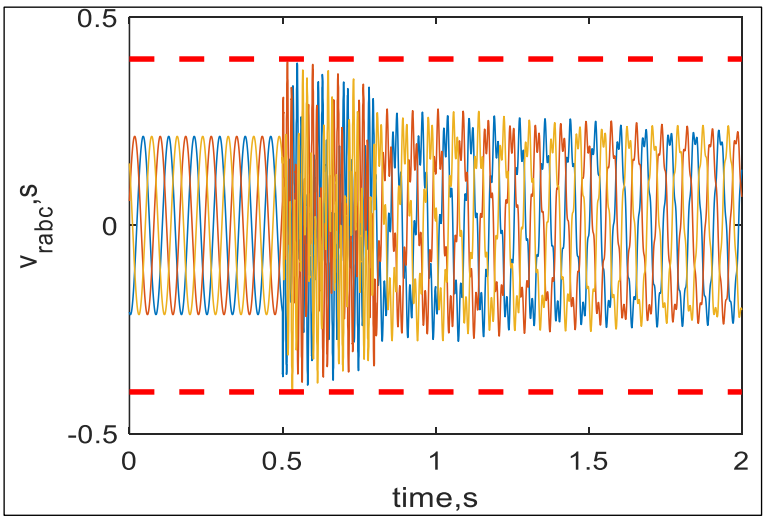


**Fig. 8.** Three phase rotor voltages using the proposed MPC controller during a small voltage dip

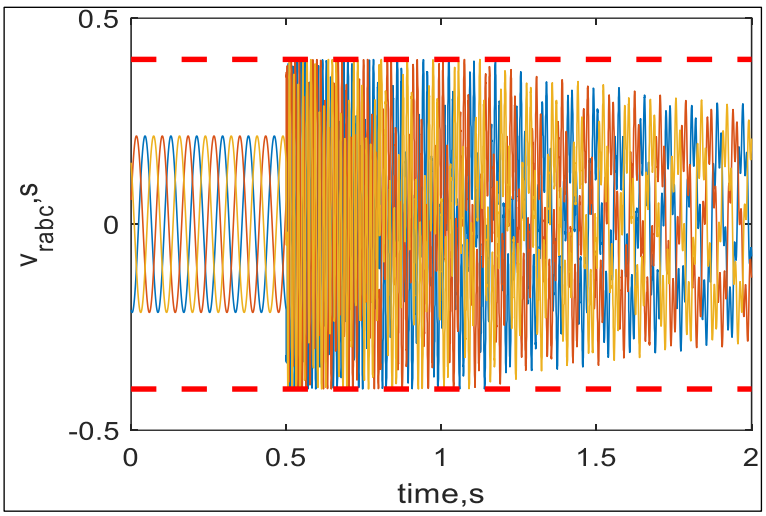


**Fig. 9.** Three-phase rotor voltages using the baseline PI controller during a small voltage dip

Fig. 9 illustrates the application of a PI controller for the stator voltage based on small voltage dips. The figure shows the PI controller applied to the same voltage dip profile. The stabilization of the stator voltage during sag mitigation took longer. Fig. 9 and Fig. 10 demonstrate the fast disturbance rejection capability of MPC.

Fig. 10 compares the performance of MPC and PI controllers for reactive power control. The reactive power output is significantly lower when using the MPC controller compared to the PI controller. The graph clearly shows that the MPC controller effectively reduces fluctuations and magnitude, whereas the PI controller shows noticeable fluctuations and higher magnitudes. The proposed MPC controller exhibits improved stability in the reactive power curve, ultimately enhancing the power quality of the DFIG.

### 5.2. Medium Voltage Dip

In the second part of the simulation (Fig. 11, Fig. 12, Fig. 13, Fig. 14, Fig. 15), a medium voltage dip of 0.5pu was applied to the WECS, and the stator current and voltage were measured after implementing the controller. Additionally, the reactive power was monitored to assess the power quality based on the MPC controller.

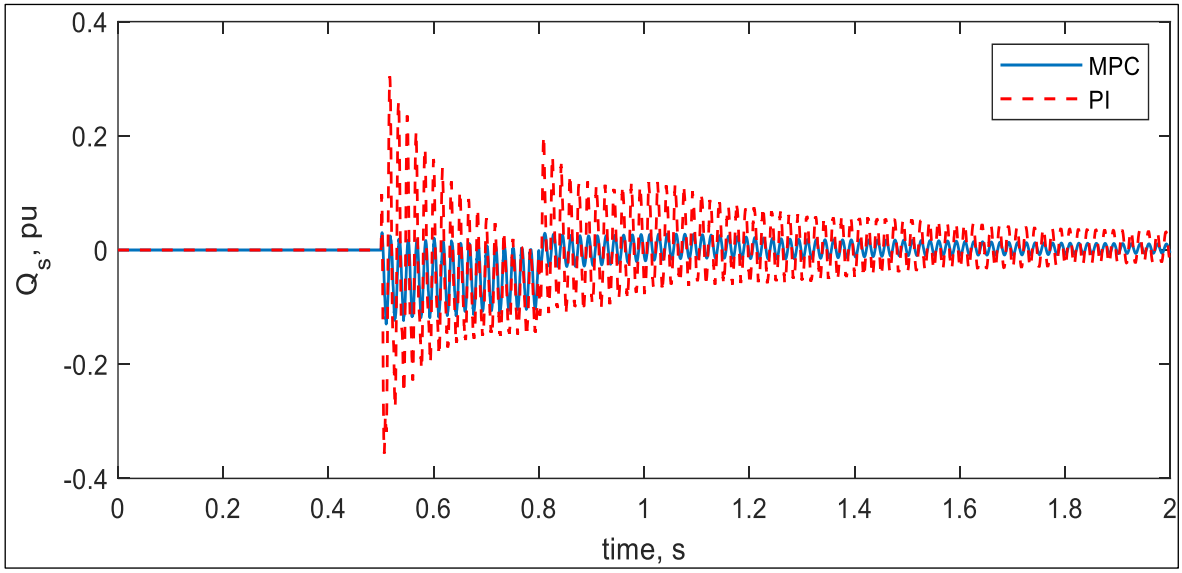


**Fig. 10.** Stator reactive power during a small voltage dip using the MPC controller (solid line) and the baseline PI controller (dashed line)

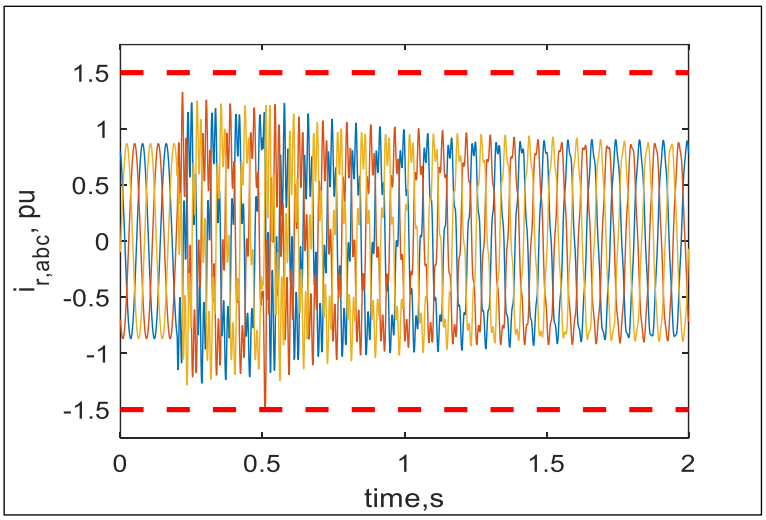


**Fig. 11.** Three-phase rotor current response using the proposed MPC controller during medium voltage dip

Fig. 11 shows the medium dip in the stator voltage of the DFIG. The current ripple increased from 0.85 to 1.25 Apu in a short period of time due to the voltage dips. However, the current quickly stabilized to reach the nominal value again. Therefore, the MPC controller can effectively protect the WECS from in-rush currents.

Fig. 12 illustrates the application of a PI controller to adjust the inrush current to the operational value. However, there is noticeable fluctuation in the inrush current due to the medium sag. The PI controller demonstrates lower efficiency performance compared to the MPC.

Fig. 13 shows the stator voltage with medium dips. The MPC controller can reach the operational value after 0.75 seconds. According to the figures, the MPC controller can adjust the voltage despite considerable disturbance caused by the medium voltage dips. However, the voltage remained within the nominal range and improved the LVRT capabilities.

Fig. 14 illustrates the application of a PI controller to the same voltage dips profile. The figure shows excessive fluctuation with significant noise, leading to a relatively high inrush current due to the behavior of the three-phase voltage fault curve.

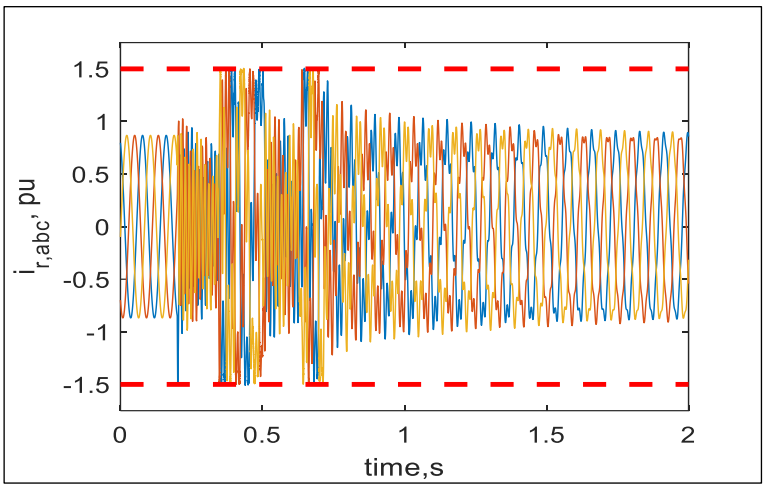


**Fig. 12.** Three-phase rotor current response using the baseline PI controller during medium voltage dip

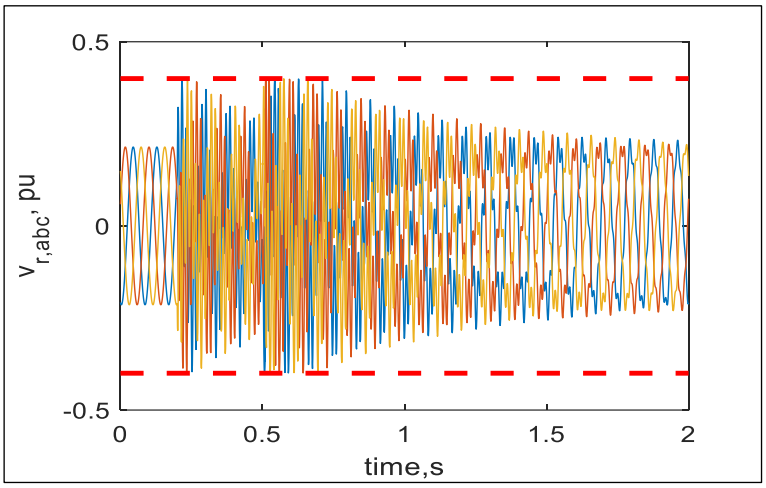


**Fig. 13.** Three-phase rotor voltages using the proposed MPC controller during medium voltage dip

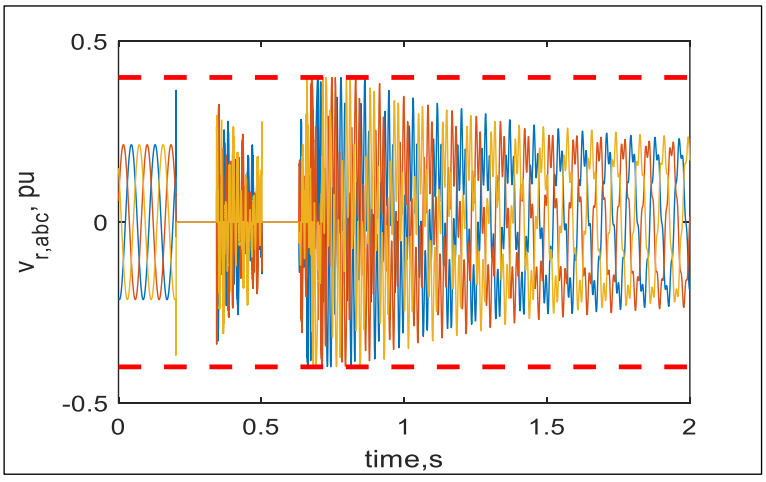


**Fig. 14.** Three-phase rotor voltages using the baseline PI controller during medium voltage dip

Fig. 15 depicts the applied MPC and PI controllers. It can be observed from the PI controller that the reactive power consumption during the fault is significantly high in the interval of (0.5-0.72) sec. In comparison, the MPC controller shows relatively stable reactive power within the interval of (0.2-0.7) sec, with only minimal fluctuations observed between (0.5-0.55) sec. The MPC controller yielded

better results in terms of the efficiency of the output stator voltage and current, ensuring the normal operation of the WECS.

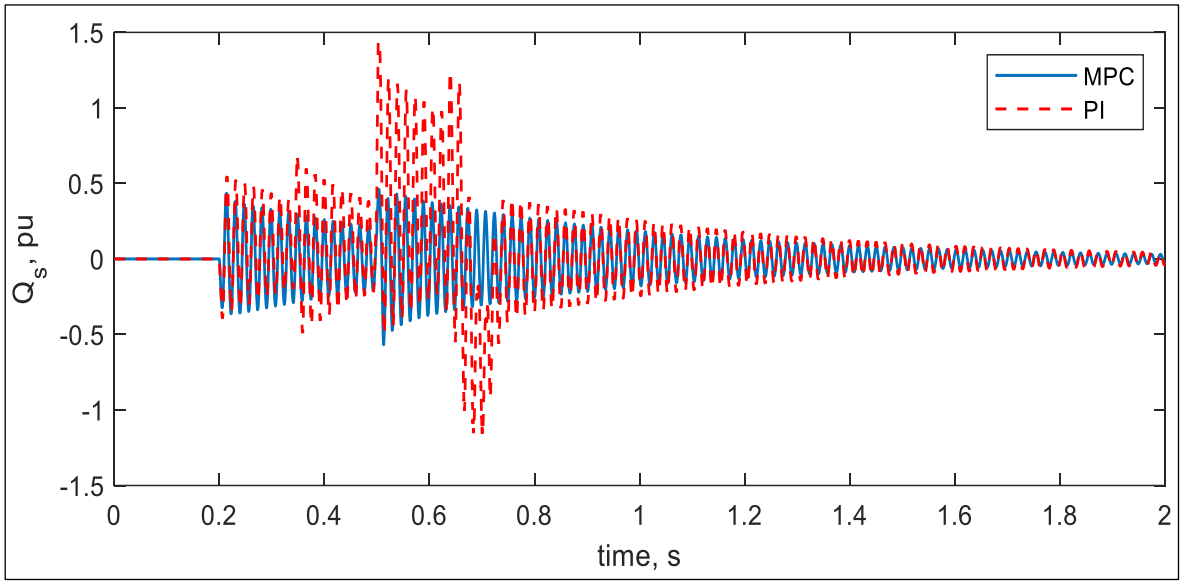


**Fig. 15.** Stator reactive power during a medium voltage dip using the MPC controller (solid line) and the baseline PI controller (dashed line)

Quantitative analysis is performed to compare the performance of the proposed MPC and the baseline PI controller. The key performance indicators are: (1) the percentage reduction in the rotor peak current, (2) the percentage reduction in the peak stator reactive power, and (3) the percentage reduction in the time taken to reject the disturbance. This will be the time from the moment of the dip until the stator reactive power is within $\pm 5\%$ of its setpoint value (0 pu). The results are summarized in Table 1. It can be concluded that the proposed MPC controller offers significant improvement to the LVRT performance of the DFIG.

The significant improvement in the LVRT performance has a strong physical implication on the stability of modern grids with large wind power penetration levels. The results in Table 1 indicate that the proposed MPC controller ensures that the DFIG wind turbine will remain connected to the grid with effective control over its reactive power for small and medium voltage dips. Consequently, when the fault is cleared, the DFIG can actively support the voltage recovery of the grid by injecting reactive power, thus increasing its stability and resiliency.

**Table 1.** Performance comparison between the proposed MPC and baseline PI controllers

| Performance Metric | Small Voltage Dip | | | Medium Voltage Dip | | |
|---|---|---|---|---|---|---|
| | MPC | PI | % Improvement | MPC | PI | % Improvement |
| Peak rotor current [pu] | 0.9 | 1.4 | 35.7% reduction | 1.35 | 1.5 | 10% reduction |
| Peak stator reactive power [pu] | 0.12 | 0.38 | 68.4% reduction | 0.45 | 1.45 | 69% reduction |
| Disturbance rejection Time [ms] | 300 | 1000 | 70% reduction | 1000 | 1700 | 41% reduction |

The main limitation of the proposed MPC controller, in comparison to the baseline PI controller, is its reliance on significant computational resources to solve the QCQP optimization problem. However, this limitation has become less significant in recent times due to the widespread availability of cost-effective computers with substantial computational power.

It is important to note that the simulations did not include the interaction between the MPC controller and the protection system (such as a crowbar or dynamic series resistance) because the rotor currents remained within safe values and the protection system was not triggered. Future research will focus on studying the interaction between the MPC controller and the protection system when the

DFIG wind turbine experiences severe voltage dips. Another potential research direction is to investigate the implementation of the proposed control strategy with PMSG wind turbines.

## 6. Conclusion

To evaluate the efficiency of the proposed MPC technique, two different approaches were used to analyze small and medium voltage dips. A comparison was conducted between the MPC controller and the conventional Proportional-Integral (PI) controller. The results show that the MPC controller outperforms the PI controller in terms of efficiency. This superiority can be attributed to several accomplishments of the MPC controller. Maintaining the current at the nominal rated value during low and medium voltage dips. Ensuring a quick response to control the voltage of the three-phase stator, thereby allowing for uniform distribution of power from the induction generator. Protecting the WECS from inrush currents and sudden surges. Maintaining the voltage within the specified range of the nominal rated value. Improving the ability to effectively withstand Low Voltage Ride Through (LVRT). Reducing sag voltage fluctuation and stabilizing current efficiently, unlike a PI controller. The simulation results of the MPC controller show that stability and disturbance rejection in sag mitigation of stator voltage require a shorter period. The MPC controller is more effective in reducing voltage ripple in the stator voltage. On the other hand, the proposed controller improves stability in the reactive power curve, enhancing the power quality of the DFIG. Moreover, the MPC controller efficiently regulates the current to achieve the desired nominal value.

**Author Contributions:** Mostafa Soliman: Methodology and simulations. Ahmed Badawi, I.M. Elzein, and Walid Alqaisi M: Data curation, writing, review and editing. All authors have read and agreed to the published version of the manuscript.

**Funding:** This research received no external funding.

**Conflicts of Interest:** The authors declare no conflict of interest.

## References

[1] R. K. Behara and A. K. Saha, "artificial intelligence control system applied in smart grid integrated doubly fed induction generator-based wind turbine: A review," *Energies*, vol. 15, no. 17, p. 6488, 2022, https://doi.org/10.3390/en15176488.

[2] A. Bensalah, G. Barakat, and Y. Amara, "Electrical generators for large wind turbine: Trends and challenges," *Energies*, vol. 15, no. 18, p. 6700, 2022, https://doi.org/10.3390/en15186700.

[3] A. M. S. Yunus, A. Abu-Siada, M. I. Mosaad, H. Albalawi, M. Aljohani and J. X. Jin, "Application of SMES Technology in Improving the Performance of a DFIG-WECS Connected to a Weak Grid," *IEEE Access*, vol. 9, pp. 124541-124548, 2021, https://doi.org/10.1109/ACCESS.2021.3110995.

[4] A. Badawi, H. Ali, N. A. Ismail, A. Zyoud, and S. H. Yusoff, "Wind energy production using novel HCS algorithm to reach MPPT for small-scale wind turbines under rapid change wind speed," *Innovation and Technological Advances for Sustainability*, pp. 183-192, 2024, https://doi.org/10.1201/9781003496724-18.

[5] A. Badawi, H. Ali, I. M. Elzein, A. Zyoud and A. Abu-Hudrouss, "Highly Efficient Pure Sine Wave Inverter Using Microcontroller for Photovoltaic Applications," *2023 International Symposium on Networks, Computers and Communications (ISNCC)*, pp. 1-6, 2023, https://doi.org/10.1109/ISNCC58260.2023.10323997.

[6] M. A. Mossa, M. K. Abdelhamid, A. A. Hassan, and N. Bianchi, "Improving the Dynamic Performance of a Variable Speed DFIG for Energy Conversion Purposes Using an Effective Control System," *Processes*, vol. 10, no. 3, p. 456, 2022, https://doi.org/10.3390/pr10030456.

[7] A. Hadoune *et al*., "Optimizing direct power control of DFIG-based WECS using super-twisting algorithm under real wind profile," *Frontiers in Energy Research*, vol. 11, p. 1261902, 2023, https://doi.org/10.3389/fenrg.2023.1261902.

[8] Z. A. Alrowaili *et al*., "Robust adaptive HCS MPPT algorithm-based wind generation system using model reference adaptive control," *Sensors*, vol. 21, no. 15, p. 5187, 2021, https://doi.org/10.3390/s21155187.

[9] A. Badawi, I. M. Elzein, H. Ali, N. Ismail, A. Zyoud and M. Soliman, "Robust Adaptive HCS MPPT Algorithm-Based Wind Generation System Using Power Prediction Mode," *2024 IEEE 8th Energy Conference (ENERGYCON)*, pp. 1-6, 2024, https://doi.org/10.1109/ENERGYCON58629.2024.10488812.

[10] A. Bakbak *et al*., "PMSG-Based Dual-Port Wind-Energy Conversion System With Reduced Converter Size," *IEEE Access*, vol. 9, pp. 118953-118967, 2021, https://doi.org/10.1109/ACCESS.2021.3107595.

[11] R. A. Ibrahim and N. E. Zakzouk, "A PMSG wind energy system featuring low-voltage ride-through via mode-shift control," *Applied sciences*, vol. 12, no. 3, p. 964, 2022, https://doi.org/10.3390/app12030964.

[12] A. S. Badawi, M. Ouda, A. Zyoud and S. H. Yusoff, "The Simplest Estimation Method of Weibull Probability Distribution Parameters," *2021 6th IEEE International Conference on Recent Advances and Innovations in Engineering (ICRAIE)*, pp. 1-5, 2021, https://doi.org/10.1109/ICRAIE52900.2021.9703996.

[13] F. K. Moghadam and A. R. Nejad, "Evaluation of PMSG-based drivetrain technologies for 10-MW floating offshore wind turbines: Pros and cons in a life cycle perspective," *Wind Energy*, vol. 23, no. 7, pp. 1542-1563, 2020, https://doi.org/10.1002/we.2499.

[14] G. E. Barter, L. Sethuraman, P. Bortolotti, J. Keller, and D. A. Torrey, "Beyond 15 MW: A cost of energy perspective on the next generation of drivetrain technologies for offshore wind turbines," *Applied Energy*, vol. 344, p. 121272, 2023, https://doi.org/10.1016/j.apenergy.2023.121272.

[15] A. S. Badawi, M. Ouda, A. Zyoud and S. H. a. Yusoff, "Maximum Power Point Tracking Controller Technique Using Permanent Magnet Synchronous Generator," *2021 6th IEEE International Conference on Recent Advances and Innovations in Engineering (ICRAIE)*, pp. 1-5, 2021, https://doi.org/10.1109/ICRAIE52900.2021.9703978.

[16] M. M. Mahmoud *et al*., "Evaluation and Comparison of Different Methods for Improving Fault Ride-Through Capability in Grid-Tied Permanent Magnet Synchronous Wind Generators," *International Transactions on Electrical Energy Systems*, vol. 2023, no. 1, p. 7717070, 2023, https://doi.org/10.1155/2023/7717070.

[17] R. Hiremath and T. Moger, "Comprehensive review on low voltage ride through capability of wind turbine generators," *International Transactions on Electrical Energy Systems*, vol. 30, no. 10, p. e12524, 2020, https://doi.org/10.1002/2050-7038.12524.

[18] P. Verma, S. K, and B. Dwivedi, "Comprehensive investigation on doubly fed induction generator-wind farms at fault ride through capabilities: Technical difficulties and improvisations," *Energy Sources, Part A: Recovery, Utilization, and Environmental Effects*, pp. 1-33, 2021, https://doi.org/10.1080/15567036.2020.1857476.

[19] J. Tait, S. Wang, K. Ahmed, and G. P. Adam, "Comparative assessment of four low voltage fault ride through techniques (LVFRT) for wind energy conversion systems (WECSs)," *Alexandria Engineering Journal*, vol. 61, no. 12, pp. 10463-10476, 2022, https://doi.org/10.1016/j.aej.2022.04.003.

[20] Y. Zhao, C. Wei, Z. Zhang and W. Qiao, "A Review on Position/Speed Sensorless Control for Permanent-Magnet Synchronous Machine-Based Wind Energy Conversion Systems," *IEEE Journal of Emerging and Selected Topics in Power Electronics*, vol. 1, no. 4, pp. 203-216, 2013, https://doi.org/10.1109/JESTPE.2013.2280572.

[21] A. Badawi *et al*., "Data bank: nine numerical methods for determining the parameters of weibull for wind energy generation tested by five statistical tools," *International Journal of Power Electronics and Drive Systems (IJPEDS)*, vol. 12, no. 2, pp. 1114-1130, 2021, http://doi.org/10.11591/ijpeds.v12.i2.pp1114-1130.

[22] A. S. Badawi, N. F. Hasbullah, S. H. Yusoff, A. Hashim, S. Khan and A. M. Zyoud, "Power prediction mode technique for Hill Climbing Search algorithm to reach the maximum power point tracking," *2020 2nd International Conference on Electrical, Control and Instrumentation Engineering (ICECIE)*, pp. 1-7, 2020, https://doi.org/10.1109/ICECIE50279.2020.9309564.

[23] A. S. Badawi, N. F. Hasbullah, S. H. Yusoff, A. Hashim, S. Khan and A. M. Zyoud, "Paper review: maximum power point tracking for wind energy conversion system," *2020 2nd International Conference on Electrical, Control and Instrumentation Engineering (ICECIE)*, pp. 1-6, 2020, https://doi.org/10.1109/ICECIE50279.2020.9309567.

[24] B. Desalegn, D. Gebeyehu, and B. Tamrat, "Wind energy conversion technologies and engineering approaches to enhancing wind power generation: A review," *Heliyon*, vol. 8, no. 11, p. e11263, 2022, https://doi.org/10.1016/j.heliyon.2022.e11263.

[25] S. Tripathi, A. Tiwari, and D. Singh, "Grid-integrated permanent magnet synchronous generator based wind energy conversion systems: A technology review," *Renewable and Sustainable Energy Reviews*, vol. 51, pp. 1288-1305, 2015, https://doi.org/10.1016/j.rser.2015.06.060.

[26] J. Pande, P. Nasikkar, K. Kotecha, V. Varadarajan, "A review of maximum power point tracking algorithms for wind energy conversion systems," *Journal of Marine Science and Engineering*, vol. 9, no. 11, p. 1187, 2021, https://doi.org/10.3390/jmse9111187.

[27] A. Badawi, S. Kazmi, R. Boby, M. Shah, and K. Matter, "Resonant circuit response for contactless energy transfer under variable PWM," *International Journal of Information and Electronics Engineering*, vol. 7, no. 1, pp. 41-47, 2017, https://doi.org/10.18178/IJIEE.2017.7.1.659.

[28] V. Yaramasu, A. Dekka, M. J. Durán, S. Kouro, and B. Wu, "PMSG-based wind energy conversion systems: survey on power converters and controls," *IET Electric Power Applications*, vol. 11, no. 6, pp. 956-968, 2017, https://doi.org/10.1049/iet-epa.2016.0799.

[29] M. Bajaj and A. K. Singh, "Grid integrated renewable DG systems: A review of power quality challenges and state-of-the-art mitigation techniques," *International Journal of Energy Research*, vol. 44, no. 1, pp. 26-69, 2020, https://doi.org/10.1002/er.4847.

[30] A. Darwish and G. A. Aggidis, "A Review on Power Electronic Topologies and Control for Wave Energy Converters," *Energies*, vol. 15, no. 23, p. 9174, 2022, https://doi.org/10.3390/en15239174.

[31] D. L. O'Sullivan and A. W. Lewis, "Generator Selection and Comparative Performance in Offshore Oscillating Water Column Ocean Wave Energy Converters," *IEEE Transactions on Energy Conversion*, vol. 26, no. 2, pp. 603-614, 2011, https://doi.org/10.1109/TEC.2010.2093527.

[32] C. Dincan, P. Kjaer, Y. -h. Chen, S. Munk-Nielsen and C. L. Bak, "A High-Power, Medium-Voltage, Series-Resonant Converter for DC Wind Turbines," *IEEE Transactions on Power Electronics*, vol. 33, no. 9, pp. 7455-7465, 2018, https://doi.org/10.1109/TPEL.2017.2770220.

[33] Q. Wei, B. Wu, D. Xu and N. R. Zargari, "A New Configuration Using PWM Current Source Converters in Low-Voltage Turbine-Based Wind Energy Conversion Systems," *IEEE Journal of Emerging and Selected Topics in Power Electronics*, vol. 6, no. 2, pp. 919-929, 2018, https://doi.org/10.1109/JESTPE.2017.2748281.

[34] A. Badawi *et al.*, "Weibull probability distribution based on four years wind speed data using nine numerical methods," *Innovation and Technological Advances for Sustainability*, pp. 193-200, 2024, https://doi.org/10.1201/9781003496724-19.

[35] A. Badawi, N. F. Hasbullah, S. H. Yusoff, H. Aisha, and A. Zyoud, "Novel technique for hill climbing search to reach maximum power point tracking," *International Journal of Power Electronics and Drive Systems (IJPEDS)*, vol. 11, no. 4, pp. 2019-2029, 2020, http://doi.org/10.11591/ijpeds.v11.i4.pp2019-2029.

[36] J. M. Carrasco *et al.*, "Power-Electronic Systems for the Grid Integration of Renewable Energy Sources: A Survey," *IEEE Transactions on Industrial Electronics*, vol. 53, no. 4, pp. 1002-1016, 2006, https://doi.org/10.1109/TIE.2006.878356.

[37] A. D. Hansen and G. Michalke, "Multi-pole permanent magnet synchronous generator wind turbines' grid support capability in uninterrupted operation during grid faults," *IET Renewable Power Generation*, vol. 3, no. 3, pp. 333-348, 2009, https://doi.org/10.1049/iet-rpg.2008.0055.

[38] F. Mwasilu, J. Justo, K.-S. Ro, and J.-W. Jung, "Improvement of dynamic performance of doubly fed induction generator-based wind turbine power system under an unbalanced grid voltage condition," *IET Renewable Power Generation*, vol. 6, no. 6, pp. 424-434, 2012, https://doi.org/10.1049/iet-rpg.2012.0110.

[39] H. E. M. Lopez, "Maximum power tracking control scheme for wind generator systems," *Texas A & M University College Station*, 2008, https://oaktrust.library.tamu.edu/server/api/core/bitstreams/156fdc8a-8a53-4dad-a4dd-41526b21f507/content.

[40] M. M. Kabsha and Z. H. Rather, "Advanced LVRT Control Scheme for Offshore Wind Power Plant," *IEEE Transactions on Power Delivery*, vol. 36, no. 6, pp. 3893-3902, 2021, https://doi.org/10.1109/TPWRD.2021.3050986.

[41] D. Xie, Z. Xu, L. Yang, J. Østergaard, Y. Xue and K. P. Wong, "A Comprehensive LVRT Control Strategy for DFIG Wind Turbines With Enhanced Reactive Power Support," *IEEE Transactions on Power Systems*, vol. 28, no. 3, pp. 3302-3310, 2013, https://doi.org/10.1109/TPWRS.2013.2240707.

[42] S. A. E. M. Ardjoun, M. Denai, and M. Abid, "A robust power control strategy to enhance LVRT capability of grid-connected DFIG-based wind energy systems," *Wind Energy*, vol. 22, no. 6, pp. 834-847, 2019, https://doi.org/10.1002/we.2325.

[43] C. Abbey and G. Joos, "Effect of low voltage ride through (LVRT) characteristic on voltage stability," *IEEE Power Engineering Society General Meeting, 2005*, vol. 2, pp. 1901-1907, 2005, https://doi.org/10.1109/PES.2005.1489659.

[44] J. Mohammadi, S. Afsharnia, E. Ebrahimzadeh, and F. Blaabjerg, "An enhanced LVRT scheme for DFIG-based WECSs under both balanced and unbalanced grid voltage sags," *Electric Power Components and Systems*, vol. 45, no. 11, pp. 1242-1252, 2017, https://doi.org/10.1080/15325008.2017.1333547.

[45] A. Bektache and B. Boukhezzar, "Nonlinear predictive control of a DFIG-based wind turbine for power capture optimization," *International journal of electrical power & Energy systems*, vol. 101, pp. 92-102, 2018, https://doi.org/10.1016/j.ijepes.2018.03.012.

[46] G. Angala Parameswari and H. Habeebullah Sait, "A comprehensive review of fault ride-through capability of wind turbines with grid-connected doubly fed induction generator," *International Transactions on Electrical Energy Systems*, vol. 30, no. 8, p. e12395, 2020, https://doi.org/10.1002/2050-7038.12395.

[47] M. Ezzat, M. Benbouzid, S. M. Muyeen and L. Harnefors, "Low-voltage ride-through techniques for DFIG-based wind turbines: state-of-the-art review and future trends," *IECON 2013 - 39th Annual Conference of the IEEE Industrial Electronics Society*, pp. 7681-7686, 2013, https://doi.org/10.1109/IECON.2013.6700413.

[48] S. Xiao, G. Yang, H. Zhou and H. Geng, "An LVRT Control Strategy Based on Flux Linkage Tracking for DFIG-Based WECS," *IEEE Transactions on Industrial Electronics*, vol. 60, no. 7, pp. 2820-2832, 2013, https://doi.org/10.1109/TIE.2012.2205354.

[49] J. Hu, B. Wang, W. Wang, H. Tang, Y. Chi and Q. Hu, "Small Signal Dynamics of DFIG-Based Wind Turbines During Riding Through Symmetrical Faults in Weak AC Grid," *IEEE Transactions on Energy Conversion*, vol. 32, no. 2, pp. 720-730, 2017, https://doi.org/10.1109/TEC.2017.2655540.

[50] V. Le, X. Li, Y. Li, T. L. T. Dong, and C. Le, "An innovative control strategy to improve the fault ride-through capability of DFIGs based on wind energy conversion systems," *Energies*, vol. 9, no. 2, p. 69, 2016, https://doi.org/10.3390/en9020069.

[51] M. Yadav, N. Pal, and D. K. Saini, "Low voltage ride through capability for resilient electrical distribution system integrated with renewable energy resources," *Energy Reports*, vol. 9, pp. 833-858, 2023, https://doi.org/10.1016/j.egyr.2022.12.023.

[52] R. A. Jerin A, P. Kaliannan, and U. Subramaniam, "Testing of low-voltage ride through capability compliance of wind turbines–a review," *International Journal of Ambient Energy*, vol. 39, no. 8, pp. 891-897, 2018, https://doi.org/10.1080/01430750.2017.1340337.

[53] S. Mali, S. James, and I. Tank, "Improving low voltage ride-through capabilities for grid connected wind turbine generator," *Energy Procedia*, vol. 54, pp. 530-540, 2014, https://doi.org/10.1016/j.egypro.2014.07.294.

[54] J. Wachter, L. Gröll and V. Hagenmeyer, "Survey of Real-World Grid Incidents–Opportunities, Arising Challenges and Lessons Learned for the Future Converter Dominated Power System," *IEEE Open Journal of Power Electronics*, vol. 5, pp. 50-69, 2024, https://doi.org/10.1109/OJPEL.2023.3343167.

[55] G. Van Kuik *et al*., "Long-term research challenges in wind energy–a research agenda by the European Academy of Wind Energy," *Wind energy science*, vol. 1, no. 1, pp. 1-39, 2016, https://doi.org/10.5194/wes-1-1-2016.

[56] P. K. Srivastava, A. N. Tiwari, and S. N. Singh, "Impacts of Wind Energy Integration to the Utility Grid and Grid Codes: A Review," *Recent Advances in Electrical & Electronic Engineering (Formerly Recent Patents on Electrical & Electronic Engineering)*, vol. 13, no. 4, pp. 446-469, 2020, http://dx.doi.org/10.2174/2352096512666190709102957.

[57] M. Tsili and S. Papathanassiou, "A review of grid code technical requirements for wind farms," *IET Renewable power generation*, vol. 3, no. 3, pp. 308-332, 2009, https://doi.org/10.1049/iet-rpg.2008.0070.

[58] M. Huang, Y. Peng, C. K. Tse, Y. Liu, J. Sun and X. Zha, "Bifurcation and Large-Signal Stability Analysis of Three-Phase Voltage Source Converter Under Grid Voltage Dips," *IEEE Transactions on Power Electronics*, vol. 32, no. 11, pp. 8868-8879, 2017, https://doi.org/10.1109/TPEL.2017.2648119.

[59] M. Debouza and A. Al-Durra, "Grid Ancillary Services From Doubly Fed Induction Generator-Based Wind Energy Conversion System: A Review," *IEEE Access*, vol. 7, pp. 7067-7081, 2019, https://doi.org/10.1109/ACCESS.2018.2890168.

[60] Z. Din, J. Zhang, Z. Xu, Y. Zhang, and J. Zhao, "Low voltage and high voltage ride-through technologies for doubly fed induction generator system: Comprehensive review and future trends," *IET Renewable power generation*, vol. 15, no. 3, pp. 614-630, 2021, https://doi.org/10.1049/rpg2.12047.

[61] M. Soliman, O. Malik, and D. Westwick, "Ensuring fault ride through for wind turbines with doubly fed induction generator: a model predictive control approach," *IFAC Proceedings Volumes*, vol. 44, no. 1, pp. 1710-1715, 2011, https://doi.org/10.3182/20110828-6-IT-1002.03060.

[62] J. Lopez, P. Sanchis, X. Roboam and L. Marroyo, "Dynamic Behavior of the Doubly Fed Induction Generator During Three-Phase Voltage Dips," *IEEE Transactions on Energy Conversion*, vol. 22, no. 3, pp. 709-717, 2007, https://doi.org/10.1109/TEC.2006.878241.

[63] J. M. Maciejowski, "Modelling and predictive control: Enabling technologies for reconfiguration," *Annual reviews in Control*, vol. 23, pp. 13-23, 1999, https://doi.org/10.1016/S1367-5788(99)90051-2.

[64] J. F. Sturm and S. Zhang, "Symmetric primal-dual path-following algorithms for semidefinite programming," *Applied Numerical Mathematics*, vol. 29, no. 3, pp. 301-315, 1999, https://doi.org/10.1016/S0168-9274(98)00099-3.

[65] A. G. Wills, G. Knagge and B. Ninness, "Fast Linear Model Predictive Control Via Custom Integrated Circuit Architecture," *IEEE Transactions on Control Systems Technology*, vol. 20, no. 1, pp. 59-71, 2012, https://doi.org/10.1109/TCST.2010.2096224.

[66] J. Benford and R. Driver, "Public attitudes to inflation and interest rates," *Bank of England Quarterly Bulletin*, vol. 48, no. 2, p. 148, 2008, https://openurl.ebsco.com/EPDB%3Agcd%3A16%3A9770352.

[67] M. Kvasnica, P. Grieder, M. Baotić, and M. Morari, "Multi-parametric toolbox (MPT)," *Hybrid Systems: Computation and Control*, pp. 448-462, 2004, https://doi.org/10.1007/978-3-540-24743-2_30.